
A-NICE-MC: Adversarial Training for MCMC

Jiaming Song
 Stanford University
 tsong@cs.stanford.edu

Shengjia Zhao
 Stanford University
 zhaosj12@cs.stanford.edu

Stefano Ermon
 Stanford University
 ermon@cs.stanford.edu

Abstract

Existing Markov Chain Monte Carlo (MCMC) methods are either based on general-purpose and domain-agnostic schemes, which can lead to slow convergence, or problem-specific proposals hand-crafted by an expert. In this paper, we propose A-NICE-MC, a novel method to automatically design efficient Markov chain kernels tailored for a specific domain. First, we propose an efficient likelihood-free adversarial training method to train a Markov chain and mimic a given data distribution. Then, we leverage flexible volume preserving flows to obtain parametric kernels for MCMC. Using a bootstrap approach, we show how to train efficient Markov chains to sample from a prescribed posterior distribution by iteratively improving the quality of both the model and the samples. Empirical results demonstrate that A-NICE-MC combines the strong guarantees of MCMC with the expressiveness of deep neural networks, and is able to significantly outperform competing methods such as Hamiltonian Monte Carlo.

1 Introduction

Variational inference (VI) and Monte Carlo (MC) methods are two key approaches to deal with complex probability distributions in machine learning. The former approximates an intractable distribution by solving a variational optimization problem to minimize a divergence measure with respect to some tractable family. The latter approximates a complex distribution using a small number of typical states, obtained by sampling ancestrally from a proposal distribution or iteratively using a suitable Markov chain (Markov Chain Monte Carlo, or MCMC).

Recent progress in deep learning has vastly advanced the field of variational inference. Notable examples include black-box variational inference and variational autoencoders [1–3], which enabled variational methods to benefit from the expressive power of deep neural networks, and adversarial training [4, 5], which allowed the training of new families of implicit generative models with efficient ancestral sampling. MCMC methods, on the other hand, have not benefited as much from these recent advancements. Unlike variational approaches, MCMC methods are iterative in nature and do not naturally lend themselves to the use of expressive function approximators [6, 7]. Even evaluating an existing MCMC technique is often challenging, and natural performance metrics are intractable to compute [8–11]. Defining an objective to improve the performance of MCMC that can be easily optimized in practice over a large parameter space is itself a difficult problem [12, 13].

To address these limitations, we introduce A-NICE-MC, a new method for training flexible MCMC kernels, e.g., parameterized using (deep) neural networks. Given a kernel, we view the resulting Markov Chain as an implicit generative model, i.e., one where sampling is efficient but evaluating the (marginal) likelihood is intractable. We then propose adversarial training as an effective, likelihood-free method for training a Markov chain to match a target distribution. First, we show it can be used in a learning setting to directly approximate an (empirical) data distribution. We then use the approach to train a Markov Chain to sample efficiently from a model prescribed by an analytic expression (e.g., a Bayesian posterior distribution), the classic use case for MCMC techniques. We leverage flexible volume preserving flow models [14] and a “bootstrap” technique to automatically design powerful

domain-specific proposals that combine the guarantees of MCMC and the expressiveness of neural networks. Finally, we propose a method that decreases autocorrelation and increases the effective sample size of the chain as training proceeds. We demonstrate that these trained operators are able to significantly outperform traditional ones, such as Hamiltonian Monte Carlo, in various domains.

2 Notations and Problem Setup

A sequence of continuous random variables $\{x_t\}_{t=0}^{\infty}$, $x_t \in \mathbb{R}^n$, is drawn through the following Markov chain:

$$x_0 \sim \pi^0 \quad x_{t+1} \sim T_{\theta}(x_{t+1}|x_t)$$

where $T_{\theta}(\cdot|x)$ is a time-homogeneous stochastic transition kernel parametrized by $\theta \in \Theta$ and π^0 is some initial distribution for x_0 . In particular, we assume that T_{θ} is defined through an implicit generative model $f_{\theta}(\cdot|x, v)$, where $v \sim p(v)$ is an auxiliary random variable, and f_{θ} is a deterministic transformation (e.g., a neural network). Let π_{θ}^t denote the distribution for x_t . If the Markov chain is both irreducible and positive recurrent, then it has an unique stationary distribution $\pi_{\theta} = \lim_{t \rightarrow \infty} \pi_{\theta}^t$. We assume that this is the case for all the parameters $\theta \in \Theta$.

Let $p_d(x)$ be a target distribution over $x \in \mathbb{R}^n$, e.g, a data distribution or an (intractable) posterior distribution in a Bayesian inference setting. Our objective is to find a T_{θ} such that:

1. **Low bias:** The stationary distribution is close to the target distribution (minimize $|\pi_{\theta} - p_d|$).
2. **Efficiency:** $\{\pi_{\theta}^t\}_{t=0}^{\infty}$ converges quickly (minimize t such that $|\pi_{\theta}^t - p_d| < \delta$).
3. **Low variance:** Samples from one chain $\{x_t\}_{t=0}^{\infty}$ should be as uncorrelated as possible (minimize autocorrelation of $\{x_t\}_{t=0}^{\infty}$).

We think of π_{θ} as a stochastic generative model, which can be used to efficiently produce samples with certain characteristics (specified by p_d), allowing for efficient Monte Carlo estimates. We consider two settings for specifying the target distribution. The first is a *learning* setting where we do not have an analytic expression for $p_d(x)$ but we have access to typical samples $\{s_i\}_{i=1}^m \sim p_d$; in the second case we have an analytic expression for $p_d(x)$, possibly up to a normalization constant, but no access to samples. The two cases are discussed in Sections 3 and 4 respectively.

3 Adversarial Training for Markov Chains

Consider the setting where we have direct access to samples from $p_d(x)$. Assume that the transition kernel $T_{\theta}(x_{t+1}|x_t)$ is the following implicit generative model:

$$v \sim p(v) \quad x_{t+1} = f_{\theta}(x_t, v) \tag{1}$$

Assuming a stationary distribution $\pi_{\theta}(x)$ exists, the value of $\pi_{\theta}(x)$ is typically intractable to compute. The marginal distribution $\pi_{\theta}^t(x)$ at time t is also intractable, since it involves integration over all the possible paths (of length t) to x . However, we can directly obtain samples from π_{θ}^t , which will be close to π_{θ} if t is large enough (assuming ergodicity). This aligns well with the idea of generative adversarial networks (GANs), a likelihood free method which only requires samples from the model.

Generative Adversarial Network (GAN) [4] is a framework for training deep generative models using a two player minimax game. A generator network G generates samples by transforming a noise variable $z \sim p(z)$ into $G(z)$. A discriminator network $D(x)$ is trained to distinguish between “fake” samples from the generator and “real” samples from a given data distribution p_d . Formally, this defines the following objective (Wasserstein GAN, from [15])

$$\min_G \max_D V(D, G) = \min_G \max_D \mathbb{E}_{x \sim p_d}[D(x)] - \mathbb{E}_{z \sim p(z)}[D(G(z))] \tag{2}$$

In our setting, we could assume $p_d(x)$ is the empirical distribution from the samples, and choose $z \sim \pi^0$ and let $G_{\theta}(z)$ be the state of the Markov Chain after t steps, which is a good approximation of π_{θ} if t is large enough. However, optimization is difficult because we do not know a reasonable t in advance, and the gradient updates are expensive due to backpropagation through the entire chain.



Figure 1: Visualizing samples of π_1 to π_{50} (each row) from a model trained on the MNIST dataset. Consecutive samples can be related in label (red box), inclination (green box) or width (blue box).



Figure 2: $T_\theta(y_{t+1}|y_t)$.

Figure 3: Samples of π_1 to π_{30} from models (top: without shortcut connections; bottom: with shortcut connections) trained on the CelebA dataset.

Therefore, we propose a more efficient approximation, called *Markov GAN* (MGAN):

$$\min_{\theta} \max_D \mathbb{E}_{x \sim p_d}[D(x)] - \lambda \mathbb{E}_{\bar{x} \sim \pi_\theta^b}[D(\bar{x})] - (1 - \lambda) \mathbb{E}_{x_d \sim p_d, \bar{x} \sim T_\theta^m(\bar{x}|x_d)}[D(\bar{x})] \quad (3)$$

where $\lambda \in (0, 1)$, $b \in \mathbb{N}^+$, $m \in \mathbb{N}^+$ are hyperparameters, \bar{x} denotes “fake” samples from the generator and $T_\theta^m(x|x_d)$ denotes the distribution of x when the transition kernel is applied m times, starting from some “real” sample x_d .

We use two types of samples from the generator for training, optimizing θ such that the samples will fool the discriminator:

1. Samples obtained after b transitions $\bar{x} \sim \pi_\theta^b$, starting from $x_0 \sim \pi^0$.
2. Samples obtained after m transitions, starting from a data sample $x_d \sim p_d$.

Intuitively, the first condition encourages the Markov Chain to converge towards p_d over relatively short runs (of length b). The second condition enforces that p_d is a fixed point for the transition operator.¹ Instead of simulating the chain until convergence, which will be especially time-consuming if the initial Markov chain takes many steps to mix, the generator would run only $(b + m)/2$ steps on average. Empirically, we observe better training times by uniformly sampling b from $[1, B]$ and m from $[1, M]$ respectively in each iteration, so we use B and M as the hyperparameters for our experiments.

3.1 Example: Generative Model for Images

We experiment with a distribution p_d over images, such as digits (MNIST) and faces (CelebA). In the experiments, we parametrize f_θ to have an autoencoding structure, where the auxiliary variable $v \sim \mathcal{N}(0, I)$ is directly added to the latent code of the network serving as a source of randomness:

$$z = \text{encoder}_\theta(x_t) \quad z' = \text{ReLU}(z + \beta v) \quad x_{t+1} = \text{decoder}_\theta(z') \quad (4)$$

where β is a hyperparameter we set to 0.1. While sampling is inexpensive, evaluating probabilities according to $T_\theta(\cdot|x_t)$ is generally intractable as it would require integration over v . The starting distribution π_0 is a factored Gaussian distribution with mean and standard deviation being the mean and standard deviation of the training set. We include all the details, which are based on the DCGAN [16] architecture, in Appendix E.1. All the models are trained with the gradient penalty objective for Wasserstein GANs [17, 15], where $\lambda = 1/3$, $B = 4$ and $M = 3$.

We visualize the samples generated from our trained Markov chain in Figures 1 and 3, where each row shows consecutive samples from the same chain (we include more images in Appendix F). From

¹We provide a more rigorous justification in Appendix B.

Figure 1 it is clear that x_{t+1} is related to x_t in terms of high-level properties such as digit identity (label). Our model learns to find and “move between the modes” of the dataset, instead of generating a single sample ancestrally. This is drastically different from other iterative generative models trained with maximum likelihood, such as Generative Stochastic Networks (GSN, [18]) and Infusion Training (IF, [19]), because when we train $T_\theta(x_{t+1}|x_t)$ we are not specifying a particular target for x_{t+1} . In fact, to maximize the discriminator score the model (generator) may choose to generate some x_{t+1} near a different mode.

To further investigate the frequency of various modes in the stationary distribution, we consider the class-to-class transition probabilities for MNIST. We run one step of the transition operator starting from real samples where we have class labels $y \in \{0, \dots, 9\}$, and classify the generated samples with a CNN. We are thus able to quantify the transition matrix for labels in Figure 2. Results show that class probabilities are fairly uniform and range between 0.09 and 0.11.

Although it seems that the MGAN objective encourages rapid transitions between different modes, it is not always the case. In particular, as shown in Figure 3, adding residual connections [20] and highway connections [21] to an existing model can significantly increase the time needed to transition between modes. This suggests that the time needed to transition between modes can be affected by the architecture we choose for $f_\theta(x_t, v)$. If the architecture introduces an information bottleneck which forces the model to “forget” x_t , then x_{t+1} will have higher chance to occur in another mode; on the other hand, if the model has shortcut connections, it tends to generate x_{t+1} that are close to x_t . The increase in autocorrelation will hinder performance if samples are used for Monte Carlo estimates.

4 Adversarial Training for Markov Chain Monte Carlo

We now consider the setting where the target distribution p_d is specified by an analytic expression:

$$p_d(x) \propto \exp(-U(x)) \quad (5)$$

where $U(x)$ is a known “energy function” and the normalization constant in Equation (5) might be intractable to compute. This form is very common in Bayesian statistics [22], computational physics [23] and graphics [24]. Compared to the setting in Section 3, there are two additional challenges:

1. We want to train a Markov chain such that the stationary distribution π_θ is *exactly* p_d ;
2. We do not have direct access to samples from p_d during training.

4.1 Exact Sampling Through MCMC

We use ideas from the Markov Chain Monte Carlo (MCMC) literature to satisfy the first condition and guarantee that $\{\pi_\theta^t\}_{t=0}^\infty$ will asymptotically converge to p_d . Specifically, we require the transition operator $T_\theta(\cdot|x)$ to satisfy the *detailed balance* condition:

$$p_d(x)T_\theta(x'|x) = p_d(x')T_\theta(x|x') \quad (6)$$

for all x and x' . This condition can be satisfied using Metropolis-Hastings (MH), where a sample x' is first obtained from a *proposal distribution* $g_\theta(x'|x)$ and accepted with the following probability:

$$A_\theta(x'|x) = \min \left(1, \frac{p_d(x')}{p_d(x)} \frac{g_\theta(x|x')}{g_\theta(x'|x)} \right) = \min \left(1, \exp(U(x) - U(x')) \frac{g_\theta(x|x')}{g_\theta(x'|x)} \right) \quad (7)$$

Therefore, the resulting MH transition kernel can be expressed as $T_\theta(x'|x) = g_\theta(x'|x)A_\theta(x'|x)$ (if $x \neq x'$), and it can be shown that p_d is stationary for $T_\theta(\cdot|x)$ [25].

The idea is then to optimize for a good proposal $g_\theta(x'|x)$. We can set g_θ directly as in Equation (1) (if f_θ takes a form where the probability g_θ can be computed efficiently), and attempt to optimize the MGAN objective in Eq. (3) (assuming we have access to samples from p_d , a challenge we will address later). Unfortunately, Eq. (7) is not differentiable - the setting is similar to policy gradient optimization in reinforcement learning. In principle, score function gradient estimators (such as REINFORCE [26]) could be used in this case; in our experiments, however, this approach leads to extremely low acceptance rates. This is because during initialization, the ratio $g_\theta(x|x')/g_\theta(x'|x)$ can be extremely low, which leads to low acceptance rates and trajectories that are not informative for training. While it might be possible to optimize directly using more sophisticated techniques from the RL literature, we introduce an alternative approach based on volume preserving dynamics.

4.2 Hamiltonian Monte Carlo and Volume Preserving Flow

To gain some intuition to our method, we introduce Hamiltonian Monte Carlo (HMC) and volume preserving flow models [27]. HMC is a widely applicable MCMC method that introduces an auxiliary “velocity” variable v to $g_\theta(x'|x)$. The proposal first draws v from $p(v)$ (typically a factored Gaussian distribution) and then obtains (x', v') by simulating the dynamics (and inverting v at the end of the simulation) corresponding to the Hamiltonian

$$H(x, v) = v^\top v / 2 + U(x) \quad (8)$$

where x and v are iteratively updated using the *leapfrog integrator* (see [27]). The transition from (x, v) to (x', v') is deterministic, invertible and volume preserving, which means that

$$g_\theta(x', v'|x, v) = g_\theta(x, v|x', v') \quad (9)$$

MH acceptance (7) is computed using the distribution $p(x, v) = p_d(x)p(v)$, where the acceptance probability is $p(x', v')/p(x, v)$ since $g_\theta(x', v'|x, v)/g_\theta(x, v|x', v') = 1$. We can safely discard v' after the transition since x and v are independent.

Let us return to the case where the proposal is parametrized by a neural network; if we could satisfy Equation 9 then we could significantly improve the acceptance rate compared to the “REINFORCE” setting. Fortunately, we can design such a proposal by using a volume preserving flow model [14].

A flow model [14, 28–30] defines a generative model for $x \in \mathbb{R}^n$ through a bijection $f : h \rightarrow x$, where $h \in \mathbb{R}^n$ have the same number of dimensions as x with a fixed prior $p_H(h)$ (typically a factored Gaussian). In this form, $p_X(x)$ is tractable because

$$p_X(x) = p_H(f^{-1}(x)) \left| \det \frac{\partial f^{-1}(x)}{\partial x} \right|^{-1} \quad (10)$$

and can be optimized by maximum likelihood.

In the case of a *volume preserving flow model* f , the determinant of the Jacobian $\frac{\partial f(h)}{\partial h}$ is one. Such models can be constructed using *additive coupling layers*, which first partition the input into two parts, y and z , and then define a mapping from (y, z) to (y', z') as:

$$y' = y \quad z' = z + m(y) \quad (11)$$

where $m(\cdot)$ can be an expressive function, such as a neural network. By stacking multiple coupling layers the model becomes highly expressive. Moreover, once we have the forward transformation f , the backward transformation f^{-1} can be easily derived. This family of models are called *Non-linear Independent Components Estimation* (NICE)[14].

4.3 A NICE Proposal

HMC has two crucial components. One is the introduction of the auxiliary variable v , which prevents random walk behavior; the other is the symmetric proposal in Equation (9), which allows the MH step to only consider $p(x, v)$. In particular, if we simulate the Hamiltonian dynamics (the deterministic part of the proposal) twice starting from any (x, v) (without MH or resampling v), we will always return to (x, v) .

Auxiliary variables can be easily integrated into neural network proposals. However, it is hard to obtain symmetric behavior. If our proposal is deterministic, then $f_\theta(f_\theta(x, v)) = (x, v)$ should hold for all (x, v) , a condition which is difficult to achieve². Therefore, we introduce a proposal which satisfies Equation (9) for any θ , while preventing random walk in practice by resampling v after every MH step.

Our proposal considers a NICE model $f_\theta(x, v)$ with its inverse f_θ^{-1} , where $v \sim p(v)$ is the auxiliary variable. We draw a sample x' from the proposal $g_\theta(x', v'|x, v)$ using the following procedure:

1. Randomly sample $v \sim p(v)$ and $u \sim \text{Uniform}[0, 1]$;
2. If $u > 0.5$, then $(x', v') = f_\theta(x, v)$;

²The cycle consistency loss (as in CycleGAN [31]) introduces a regularization term for this condition; we added this to the REINFORCE objective but were not able to achieve satisfactory results.

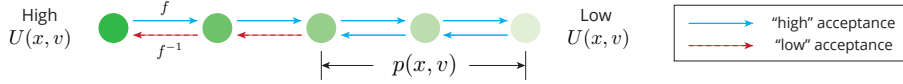


Figure 4: Sampling process of A-NICE-MC. Each step, the proposal executes f_θ or f_θ^{-1} . Outside the high probability regions f_θ will guide x towards $p_d(x)$, while MH will tend to reject f_θ^{-1} . Inside high probability regions both operations will have a reasonable probability of being accepted.

3. If $u \leq 0.5$, then $(x', v') = f_\theta^{-1}(x, v)$.

We call this proposal a *NICE proposal* and introduce the following theorem.

Theorem 1. *For any (x, v) and (x', v') in their domain, a NICE proposal g_θ satisfies*

$$g_\theta(x', v' | x, v) = g_\theta(x, v | x', v')$$

Proof. In Appendix C. □

4.4 Training A NICE Proposal

Given any NICE proposal with f_θ , the MH acceptance step guarantees that p_d is a stationary distribution, yet the ratio $p(x', v')/p(x, v)$ can still lead to low acceptance rates unless θ is carefully chosen. Intuitively, we would like to train our proposal g_θ to produce samples that are likely under $p(x, v)$.

Although the proposal itself is non-differentiable w.r.t. x and v , we do not require score function gradient estimators to train it. In fact, if f_θ is a bijection between samples in high probability regions, then f_θ^{-1} is automatically also such a bijection. Therefore, we ignore f_θ^{-1} during training and only train $f_\theta(x, v)$ to reach the target distribution $p(x, v) = p_d(x)p(v)$. For $p_d(x)$, we use the MGAN objective in Equation (3); for $p(v)$, we minimize the distance between the distribution for the generated v' (tractable through Equation (10)) and the prior distribution $p(v)$ (which is a factored Gaussian):

$$\min_{\theta} \max_D L(x; \theta, D) + \gamma L_d(p(v), p_\theta(v')) \quad (12)$$

where L is the MGAN objective, L_d is an objective that measures the divergence between two distributions and γ is a parameter to balance between the two factors; in our experiments, we use KL divergence for L_d and $\gamma = 1$ ³.

Our transition operator includes a trained NICE proposal followed by a Metropolis-Hastings step, and we call the resulting Markov chain *Adversarial NICE Monte Carlo* (A-NICE-MC). The sampling process is illustrated in Figure 4. Intuitively, if (x, v) lies in a high probability region, then both f_θ and f_θ^{-1} should propose a state in another high probability region. If (x, v) is in a low-probability probability region, then f_θ would move it closer to the target, while f_θ^{-1} does the opposite. However, the MH step will bias the process towards high probability regions, thereby suppressing the random-walk behavior.

4.5 Bootstrap

The main remaining challenge is that we do not have direct access to samples from p_d in order to train f_θ according to the adversarial objective in Equation (12), whereas in the case of Section 3, we have a dataset to get samples from the data distribution.

In order to retrieve samples from p_d and train our model, we use a bootstrap process [33] where the quality of samples used for adversarial training should increase over time. We obtain initial samples by running a (possibly) slow mixing operator T_{θ_0} with stationary distribution p_d starting from an arbitrary initial distribution π_0 . We use these samples to train our model f_{θ_i} , and then use it to obtain new samples from our trained transition operator T_{θ_i} ; by repeating the process we can obtain samples of better quality which should in turn lead to a better model.

³The results are not very sensitive to changes in γ ; we also tried Maximum Mean Discrepancy (MMD, see [32] for details) and achieved similar results.



Figure 5: *Left*: Samples from a model with shortcut connections trained with ordinary discriminator. *Right*: Samples from the same model trained with a pairwise discriminator.

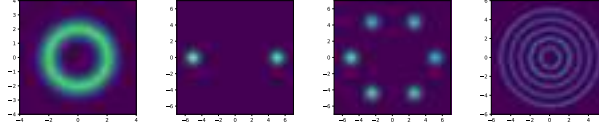


Figure 6: Densities of **ring**, **mog2**, **mog6** and **ring5** (from left to right).

4.6 Reducing Autocorrelation by Pairwise Discriminator

An important metric for evaluating MCMC algorithms is the effective sample size (ESS), which measures the number of “effective samples” we obtain from running the chain. As samples from MCMC methods are not i.i.d., to have higher ESS we would like the samples to be as independent as possible (low autocorrelation). In the case of training a NICE proposal, the objective in Equation (3) may lead to high autocorrelation even though the acceptance rate is reasonably high. This is because the coupling layer contains residual connections from the input to the output; as shown in Section 3.1, such models tend to learn an identity mapping and empirically they have high autocorrelation.

We propose to use a *pairwise discriminator* to reduce autocorrelation and improve ESS. Instead of scoring one sample at a time, the discriminator scores two samples (x_1, x_2) at a time. For “real data” we draw two independent samples from our bootstrapped samples; for “fake data” we draw $x_2 \sim T_\theta^m(\cdot|x_1)$ such that x_1 is either drawn from the data distribution or from samples after running the chain for b steps, and x_2 is the sample after running the chain for m steps, which is similar to the samples drawn in the original MGAN objective.

The optimal solution would be match both distributions of x_1 and x_2 to the target distribution. Moreover, if x_1 and x_2 are correlated, then the discriminator should be able distinguish the “real” and “fake” pairs, so the model is forced to generate samples with little autocorrelation. More details are included in Appendix D. The pairwise discriminator is conceptually similar to the minibatch discrimination layer [34]; the difference is that we provide correlated samples as “fake” data, while [34] provides independent samples that might be similar.

To demonstrate the effectiveness of the pairwise discriminator, we show an example for the image domain in Figure 5, where the same model with shortcut connections is trained with and without pairwise discrimination (details in Appendix E.1); it is clear from the variety in the samples that the pairwise discriminator significantly reduces autocorrelation.

5 Experiments

Code for reproducing the experiments is available at <https://github.com/ermongroup/a-nice-mc>.

To demonstrate the effectiveness of A-NICE-MC, we first compare its performance with HMC on several synthetic 2D energy functions: **ring** (a ring-shaped density), **mog2** (a mixture of 2 Gaussians) **mog6** (a mixture of 6 Gaussians), **ring5** (a mixture of 5 distinct rings). The densities are illustrated in Figure 6 (Appendix E.2 has the analytic expressions). *ring* has a single connected component of high-probability regions and HMC performs well; *mog2*, *mog6* and *ring5* are selected to demonstrate cases where HMC fails to move across modes using gradient information. A-NICE-MC performs well in all the cases.

We use the same hyperparameters for all the experiments (see Appendix E.4 for details). In particular, we consider $f_\theta(x, v)$ with three coupling layers, which update v , x and v respectively. This is to ensure that both x and v could affect the updates to x' and v' .

How does A-NICE-MC perform? We evaluate and compare ESS and ESS per second (ESS/s) for both methods in Table 1. For *ring*, *mog2*, *mog6*, we report the smallest ESS of all the dimensions

Table 1: Performance of MCMC samplers as measured by Effective Sample Size (ESS). Higher is better (1000 maximum). Averaged over 5 runs under different initializations. See Appendix A for the ESS formulation, and Appendix E.3 for how we benchmark the running time of both methods.

	ESS	A-NICE-MC	HMC		ESS/s	A-NICE-MC	HMC
ring	1000.00	1000.00		ring	128205	121212	
mog2	355.39	1.00		mog2	50409	78	
mog6	320.03	1.00		mog6	40768	39	
ring5	155.57	0.43		ring5	19325	29	

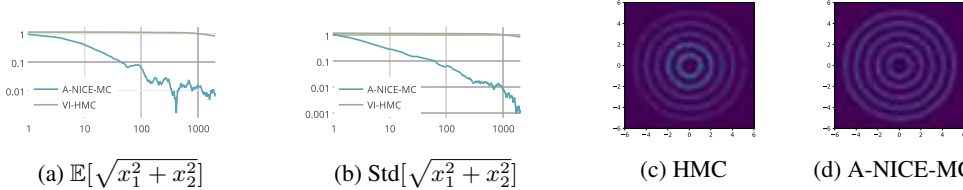


Figure 7: (a-b) Mean absolute error for estimating the statistics in *ring5* w.r.t. simulation length. Averaged over 100 chains. (c-d) Density plots for both methods. When the initial distribution is a Gaussian centered at the origin, HMC overestimates the densities of the rings towards the center.

(as in [35]); for *ring5*, we report the ESS of the distance between the sample and the origin, which indicates mixing across different rings. In the four scenarios, HMC performed well only in *ring*; in cases where modes are distant from each other, there is little gradient information for HMC to move between modes. On the other hand, A-NICE-MC is able to freely move between the modes since the NICE proposal is parametrized by a flexible neural network.

We use *ring5* as an example to demonstrate the results. We assume $\pi_0(x) = \mathcal{N}(0, \sigma^2 I)$ as the initial distribution, and optimize σ through maximum likelihood. Then we run both methods, and use the resulting particles to estimate p_d . As shown in Figures 7a and 7b, HMC fails and there is a large gap between true and estimated statistics. This also explains why the ESS is lower than 1 for HMC for *ring5* in Table 1.

Another reasonable measurement to consider is Gelman’s R hat diagnostic [36], which evaluates performance across multiple sampled chains. We evaluate this over the *rings5* domain (where the statistic is the distance to the origin), using 32 chains with 5000 samples and 1000 burn-in steps for each sample. HMC gives a R hat value of 1.26, whereas A-NICE-MC gives a R hat value of 1.002⁴. This suggests that even with 32 chains, HMC does not succeed at estimating the distribution reasonably well.

Does training increase ESS? We show in Figure 8 that in all cases ESS increases with more training iterations and bootstrap rounds, which also indicates that using the pairwise discriminator is effective at reducing autocorrelation.

Admittedly, training introduces an additional computational cost which HMC could utilize to obtain more samples initially (not taking parameter tuning into account), yet the initial cost can be amortized thanks to the improved ESS. For example, in the *ring5* domain, we can reach an ESS of 121.54 in approximately 550 seconds (2500 iterations on 1 thread CPU, bootstrap included). If we then sample from the trained A-NICE-MC, it will catch up with HMC in less than 2 seconds.

Next, we demonstrate the effectiveness of A-NICE-MC on Bayesian logistic regression, where the posterior has a single mode in a higher dimensional space, making HMC a strong candidate for the task. However, in order to achieve high ESS, HMC samplers typically use many leap frog steps and require gradients at every step, which is inefficient when $\nabla_x U(x)$ is computationally expensive. A-NICE-MC only requires running f_θ or f_θ^{-1} once to obtain a proposal, which is much cheaper computationally. We consider three datasets - *german* (25 covariates, 1000 data points), *heart* (14 covariates, 532 data points) and *australian* (15 covariates, 690 data points) - and evaluate the lowest ESS across all covariates (following the settings in [35]), where we obtain 5000 samples after 1000

⁴For R hat values, the perfect value is 1, and 1.1-1.2 would be regarded as too high.

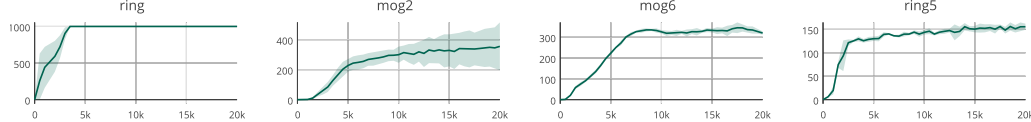


Figure 8: ESS with respect to the number of training iterations.

Table 2: ESS and ESS per second for Bayesian logistic regression tasks.

ESS	A-NICE-MC	HMC	ESS/s	A-NICE-MC	HMC
german	926.49	2178.00	german	1289.03	216.17
heart	1251.16	5000.00	heart	3204.00	1005.03
australian	1015.75	1345.82	australian	1857.37	289.11

burn-in samples. For HMC we use 40 leap frog steps and tune the step size for the best ESS possible. For A-NICE-MC we use the same hyperparameters for all experiments (details in Appendix E.5). Although HMC outperforms A-NICE-MC in terms of ESS, the NICE proposal is less expensive to compute than the HMC proposal by almost an order of magnitude, which leads to higher ESS *per second* (see Table 2).

6 Discussion

To the best of our knowledge, this paper presents the first likelihood-free method to train a parametric MCMC operator with good mixing properties. The resulting Markov Chains can be used to target both empirical and analytic distributions. We showed that using our novel training objective we can leverage flexible neural networks and volume preserving flow models to obtain domain-specific transition kernels. These kernels significantly outperform traditional ones which are based on elegant yet very simple and general-purpose analytic formulas. Our hope is that these ideas will allow us to bridge the gap between MCMC and neural network function approximators, similarly to what “black-box techniques” did in the context of variational inference [1].

Combining the guarantees of MCMC and the expressiveness of neural networks unlocks the potential to perform fast and accurate inference in high-dimensional domains, such as Bayesian neural networks. This would likely require us to gather the initial samples through other methods, such as variational inference, since the chances for untrained proposals to “stumble upon” low energy regions is diminished by the curse of dimensionality. Therefore, it would be interesting to see whether we could bypass the bootstrap process and directly train on $U(x)$ by leveraging the properties of flow models. Another promising future direction is to investigate proposals that can rapidly adapt to changes in the data. One use case is to infer the latent variable of a particular data point, as in variational autoencoders. We believe it should be possible to utilize meta-learning algorithms with data-dependent parametrized proposals.

Acknowledgements

This research was funded by Intel Corporation, TRI, FLI and NSF grants 1651565, 1522054, 1733686. The authors would like to thank Daniel Lévy for discussions on the NICE proposal proof, Yingzhen Li for suggestions on the training procedure and Aditya Grover for suggestions on the implementation.

References

- [1] R. Ranganath, S. Gerrish, and D. Blei, “Black box variational inference,” in *Artificial Intelligence and Statistics*, pp. 814–822, 2014.
- [2] D. P. Kingma and M. Welling, “Auto-encoding variational bayes,” *arXiv preprint arXiv:1312.6114*, 2013.
- [3] D. J. Rezende, S. Mohamed, and D. Wierstra, “Stochastic backpropagation and approximate inference in deep generative models,” *arXiv preprint arXiv:1401.4082*, 2014.

- [4] I. Goodfellow, J. Pouget-Abadie, M. Mirza, B. Xu, D. Warde-Farley, S. Ozair, A. Courville, and Y. Bengio, “Generative adversarial nets,” in *Advances in neural information processing systems*, pp. 2672–2680, 2014.
- [5] S. Mohamed and B. Lakshminarayanan, “Learning in implicit generative models,” *arXiv preprint arXiv:1610.03483*, 2016.
- [6] T. Salimans, D. P. Kingma, M. Welling, *et al.*, “Markov chain monte carlo and variational inference: Bridging the gap.,” in *ICML*, vol. 37, pp. 1218–1226, 2015.
- [7] N. De Freitas, P. Højen-Sørensen, M. I. Jordan, and S. Russell, “Variational mcmc,” in *Proceedings of the Seventeenth conference on Uncertainty in artificial intelligence*, pp. 120–127, Morgan Kaufmann Publishers Inc., 2001.
- [8] J. Gorham and L. Mackey, “Measuring sample quality with stein’s method,” in *Advances in Neural Information Processing Systems*, pp. 226–234, 2015.
- [9] J. Gorham, A. B. Duncan, S. J. Vollmer, and L. Mackey, “Measuring sample quality with diffusions,” *arXiv preprint arXiv:1611.06972*, 2016.
- [10] J. Gorham and L. Mackey, “Measuring sample quality with kernels,” *arXiv preprint arXiv:1703.01717*, 2017.
- [11] S. Ermon, C. P. Gomes, A. Sabharwal, and B. Selman, “Designing fast absorbing markov chains.,” in *AAAI*, pp. 849–855, 2014.
- [12] N. Mahendran, Z. Wang, F. Hamze, and N. De Freitas, “Adaptive mcmc with bayesian optimization.,” in *AISTATS*, vol. 22, pp. 751–760, 2012.
- [13] S. Boyd, P. Diaconis, and L. Xiao, “Fastest mixing markov chain on a graph,” *SIAM review*, vol. 46, no. 4, pp. 667–689, 2004.
- [14] L. Dinh, D. Krueger, and Y. Bengio, “Nice: Non-linear independent components estimation,” *arXiv preprint arXiv:1410.8516*, 2014.
- [15] M. Arjovsky, S. Chintala, and L. Bottou, “Wasserstein gan,” *arXiv preprint arXiv:1701.07875*, 2017.
- [16] A. Radford, L. Metz, and S. Chintala, “Unsupervised representation learning with deep convolutional generative adversarial networks,” *arXiv preprint arXiv:1511.06434*, 2015.
- [17] I. Gulrajani, F. Ahmed, M. Arjovsky, V. Dumoulin, and A. Courville, “Improved training of wasserstein gans,” *arXiv preprint arXiv:1704.00028*, 2017.
- [18] Y. Bengio, E. Thibodeau-Laufer, G. Alain, and J. Yosinski, “Deep generative stochastic networks trainable by backprop,” 2014.
- [19] F. Bordes, S. Honari, and P. Vincent, “Learning to generate samples from noise through infusion training,” *ICLR*, 2017.
- [20] K. He, X. Zhang, S. Ren, and J. Sun, “Deep residual learning for image recognition,” in *Proceedings of the IEEE Conference on Computer Vision and Pattern Recognition*, pp. 770–778, 2016.
- [21] R. K. Srivastava, K. Greff, and J. Schmidhuber, “Highway networks,” *arXiv preprint arXiv:1505.00387*, 2015.
- [22] P. J. Green, “Reversible jump markov chain monte carlo computation and bayesian model determination,” *Biometrika*, pp. 711–732, 1995.
- [23] W. Jakob and S. Marschner, “Manifold exploration: a markov chain monte carlo technique for rendering scenes with difficult specular transport,” *ACM Transactions on Graphics (TOG)*, vol. 31, no. 4, p. 58, 2012.

- [24] D. P. Landau and K. Binder, *A guide to Monte Carlo simulations in statistical physics*. Cambridge university press, 2014.
- [25] W. K. Hastings, “Monte carlo sampling methods using markov chains and their applications,” *Biometrika*, vol. 57, no. 1, pp. 97–109, 1970.
- [26] R. J. Williams, “Simple statistical gradient-following algorithms for connectionist reinforcement learning,” *Machine learning*, vol. 8, no. 3-4, pp. 229–256, 1992.
- [27] R. M. Neal *et al.*, “Mcmc using hamiltonian dynamics,” *Handbook of Markov Chain Monte Carlo*, vol. 2, pp. 113–162, 2011.
- [28] D. J. Rezende and S. Mohamed, “Variational inference with normalizing flows,” *arXiv preprint arXiv:1505.05770*, 2015.
- [29] D. P. Kingma, T. Salimans, and M. Welling, “Improving variational inference with inverse autoregressive flow,” *arXiv preprint arXiv:1606.04934*, 2016.
- [30] A. Grover, M. Dhar, and S. Ermon, “Flow-gan: Bridging implicit and prescribed learning in generative models,” *arXiv preprint arXiv:1705.08868*, 2017.
- [31] J.-Y. Zhu, T. Park, P. Isola, and A. A. Efros, “Unpaired image-to-image translation using cycle-consistent adversarial networks,” *arXiv preprint arXiv:1703.10593*, 2017.
- [32] Y. Li, K. Swersky, and R. Zemel, “Generative moment matching networks,” in *International Conference on Machine Learning*, pp. 1718–1727, 2015.
- [33] B. Efron and R. J. Tibshirani, *An introduction to the bootstrap*. CRC press, 1994.
- [34] T. Salimans, I. Goodfellow, W. Zaremba, V. Cheung, A. Radford, and X. Chen, “Improved techniques for training gans,” in *Advances in Neural Information Processing Systems*, pp. 2226–2234, 2016.
- [35] M. Girolami and B. Calderhead, “Riemann manifold langevin and hamiltonian monte carlo methods,” *Journal of the Royal Statistical Society: Series B (Statistical Methodology)*, vol. 73, no. 2, pp. 123–214, 2011.
- [36] S. P. Brooks and A. Gelman, “General methods for monitoring convergence of iterative simulations,” *Journal of computational and graphical statistics*, vol. 7, no. 4, pp. 434–455, 1998.
- [37] M. D. Hoffman and A. Gelman, “The no-u-turn sampler: adaptively setting path lengths in hamiltonian monte carlo.,” *Journal of Machine Learning Research*, vol. 15, no. 1, pp. 1593–1623, 2014.
- [38] M. Abadi, A. Agarwal, P. Barham, E. Brevdo, Z. Chen, C. Citro, G. S. Corrado, A. Davis, J. Dean, M. Devin, *et al.*, “Tensorflow: Large-scale machine learning on heterogeneous distributed systems,” *arXiv preprint arXiv:1603.04467*, 2016.
- [39] D. Kingma and J. Ba, “Adam: A method for stochastic optimization,” *arXiv preprint arXiv:1412.6980*, 2014.

A Estimating Effective Sample Size

Assume a target distribution $p(x)$, and a Markov chain Monte Carlo (MCMC) sampler that produces a set of N correlated samples $\{x_i\}_1^N$ from some distribution $q(\{x_i\}_1^N)$ such that $q(x_i) = p(x_i)$. Suppose we are estimating the mean of $p(x)$ through sampling; we assume that increasing the number of samples will reduce the variance of that estimate.

Let $V = \text{Var}_q[\sum_{i=1}^N x_i/N]$ be the variance of the mean estimate through the MCMC samples. The effective sample size (ESS) of $\{x_i\}_1^N$, which we denote as $M = ESS(\{x_i\}_1^N)$, is the number of independent samples from $p(x)$ needed in order to achieve the same variance, i.e. $\text{Var}_p[\sum_{j=1}^M x_j/M] = V$. A practical algorithm to compute the ESS given $\{x_i\}_1^N$ is provided by:

$$ESS(\{x_i\}_1^N) = \frac{N}{1 + 2 \sum_{s=1}^{N-1} (1 - \frac{s}{N}) \rho_s} \quad (13)$$

where ρ_s denotes the autocorrelation under q of x at lag s . We compute the following empirical estimate $\hat{\rho}_s$ for ρ_s :

$$\hat{\rho}_s = \frac{1}{\hat{\sigma}^2(N-s)} \sum_{n=s+1}^N (x_n - \hat{\mu})(x_{n-s} - \hat{\mu}) \quad (14)$$

where $\hat{\mu}$ and $\hat{\sigma}$ are the empirical mean and variance obtained by an independent sampler.

Due to the noise in large lags s , we adopt the approach of [37] where we truncate the sum over the autocorrelations when the autocorrelation goes below 0.05.

B Justifications for Objective in Equation 3

We consider two necessary conditions for p_d to be the stationary distribution of the Markov chain, which can be translated into a new algorithm with better optimization properties, described in Equation 3.

Proposition 1. Consider a sequence of ergodic Markov chains over state space \mathcal{S} . Define π_n as the stationary distribution for the n -th Markov chain, and π_n^t as the probability distribution at time step t for the n -th chain. If the following two conditions hold:

1. $\exists b > 0$ such that the sequence $\{\pi_n^b\}_{n=1}^\infty$ converges to p_d in total variation;
2. $\exists \epsilon > 0, \rho < 1$ such that $\exists M > 0, \forall n > M$, if $\|\pi_n^t - p_d\|_{\text{TV}} < \epsilon$, then $\|\pi_n^{t+1} - p_d\|_{\text{TV}} < \rho \|\pi_n^t - p_d\|_{\text{TV}}$;

then the sequence of stationary distributions $\{\pi_n\}_{n=1}^\infty$ converges to p_d in total variation.

Proof. The goal is to prove that $\forall \delta > 0, \exists K > 0, T > 0$, such that $\forall n > N, t > T, \|\pi_n^t - p_d\|_{\text{TV}} < \delta$.

According to the first assumption, $\exists N > 0$, such that $\forall n > N, \|\pi_n^b - p_d\|_{\text{TV}} < \epsilon$.

Therefore, $\forall n > K = \max(N, M), \forall \delta > 0, \exists T = b + \max(0, \lceil \log_\rho \delta - \log_\rho \epsilon \rceil) + 1$, such that $\forall t > T$,

$$\begin{aligned} & \|\pi_n^t - p_d\|_{\text{TV}} \\ &= \|\pi_n^b - p_d\|_{\text{TV}} \prod_{i=b}^{t-1} \frac{\|\pi_n^{i+1} - p_d\|_{\text{TV}}}{\|\pi_n^i - p_d\|_{\text{TV}}} \\ &< \epsilon \rho^{t-b} < \epsilon \rho^{T-b} < \epsilon \cdot \frac{\delta}{\epsilon} = \delta \end{aligned} \quad (15)$$

The first inequality uses the fact that $\|\pi_n^b - p_d\|_{\text{TV}} < \epsilon$ (from Assumption 1), and $\|\pi_n^{t+1} - p_d\|_{\text{TV}} / \|\pi_n^t - p_d\|_{\text{TV}} < \rho$ (from Assumption 2). The second inequality is true because $\rho < 1$ by Assumption 2. The third inequality uses the fact that $T - b > \lceil \log_\rho \delta - \log_\rho \epsilon \rceil$ (from definition of T), so $\rho^{T-b} < \delta/\epsilon$. Hence the sequence $\{\pi_n\}_{n=1}^\infty$ converges to p_d in total variation. \square

Moreover, convergence in total variation distance is equivalent to convergence in Jensen-Shannon (JS) divergence[15], which is what GANs attempt to minimize [4]. This motivates the use of GANs to achieve the two conditions in Proposition 1. This suggests a new optimization criterion, where we look for a θ that satisfies both conditions in Proposition 1, which translates to Equation 3.

C Proof of Theorem 1

Proof. For any (x, v) and (x', v') , g satisfies:

$$\begin{aligned}
g(x', v' | x, v) &= \frac{1}{2} \left| \det \frac{\partial f(x, v)}{\partial (x, v)} \right|^{-1} \mathbb{I}(x', v' = f(x, v)) + \frac{1}{2} \left| \det \frac{\partial f(x, v)}{\partial (x, v)} \right| \mathbb{I}(x', v' = f^{-1}(x, v)) \\
&= \frac{1}{2} \mathbb{I}(x', v' = f(x, v)) + \frac{1}{2} \mathbb{I}(x', v' = f^{-1}(x, v)) \\
&= \frac{1}{2} \mathbb{I}(x, v = f^{-1}(x', v')) + \frac{1}{2} \mathbb{I}(x, v = f(x', v')) \\
&= g(x, v | x', v')
\end{aligned} \tag{16}$$

where $\mathbb{I}(\cdot)$ is the indicator function, the first equality is the definition of $g(x', v' | x, v)$, the second equality is true since $f(x, v)$ is volume preserving, the third equality is a reparametrization of the conditions, and the last equality uses the definition of $g(x, v | x', v')$ and f is volume preserving, so the determinant of the Jacobian is 1. \square

Theorem 1 allows us to use the ration $p(x', v')/p(x, v)$ when performing the MH step.

D Details on the Pairwise Discriminator

Similar to the settings in MGAN objective, we consider two chains to obtain samples:

- Starting from a data point x , sample z_1 in B steps.
- Starting from some noise z , sample z_2 in B steps; and from z_2 sample z_3 in M steps.

For the “generated” (fake) data, we use two type of pairs (x, z_1) , and (z_2, z_3) . This is illustrated in Figure 9. We assume equal weights between the two types of pairs.

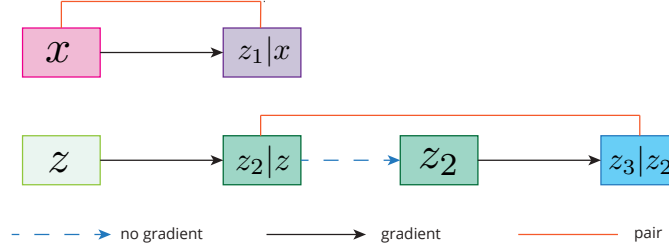


Figure 9: Illustration of the generative process for the pairwise discriminator. We block the gradient for z_2 to further parallelize the process and improve training speed.

E Additional Experimental Details

E.1 Architectures for Generative Model for Images

Code is available at <https://github.com/ermongroup/markov-chain-gan>.

Let ‘fc n , (activation)’ denote a fully connected layer with n neurons. Let ‘conv2d n, k, s , (activation)’ denote a convolutional layer with n filters of size k and stride s . Let ‘deconv2d n, k, s , (activation)’ denote a transposed convolutional layer with n filters of size k and stride s .

We use the following model to generate Figure 1 (MNIST).

encoder	decoder	discriminator
fc 600, lrelu fc 100, linear	fc 600, lrelu fc 784, sigmoid	conv2d 64, $4 \times 4, 2 \times 2$, relu conv2d 128, $4 \times 4, 2 \times 2$, lrelu fc 600, lrelu fc 1, linear

We use the following model to generate Figure 3 (CelebA, top)

encoder	decoder	discriminator
conv2d 64, $4 \times 4, 2 \times 2$, lrelu fc 200, linear	fc $16 \times 16 \times 64$, lrelu deconv2d 3, $4 \times 4, 2 \times 2$, tanh	conv2d 64, $4 \times 4, 2 \times 2$, relu conv2d 128, $4 \times 4, 2 \times 2$, lrelu conv2d 256, $4 \times 4, 2 \times 2$, lrelu fc 1, linear

For the bottom figure in Figure 3, we add a residual connection such that the input to the second layer of the decoder is the sum of the outputs from the first layers of the decoder and encoder (both have shape $16 \times 16 \times 64$); we add a highway connection from input image to the output of the decoder:

$$\bar{x} = \alpha x + (1 - \alpha)\hat{x}$$

where \bar{x} is the output of the function, \hat{x} is the output of the decoder, and α is an additional transposed convolutional output layer with sigmoid activation that has the same dimension as \hat{x} .

We use the following model to generate Figure 5 (CelebA, pairwise):

encoder	decoder	discriminator
conv2d 64, $4 \times 4, 2 \times 2$, lrelu	fc 1024, relu	conv2d 64, $4 \times 4, 2 \times 2$, relu
conv2d 64, $4 \times 4, 2 \times 2$	fc $8 \times 8 \times 128$, relu	conv2d 128, $4 \times 4, 2 \times 2$, lrelu
fc 1024, lrelu	deconv2d 64, $4 \times 4, 2 \times 2$, relu	conv2d 256, $4 \times 4, 2 \times 2$, lrelu
fc 200 linear	deconv2d 3, $4 \times 4, 2 \times 2$, tanh	fc 1, linear

For the pairwise discriminator, we double the number of filters in each convolutional layer. According to [17], we only use batch normalization in the generator for all experiments.

E.2 Analytic Forms of Energy Functions

Let $f(x|\mu, \sigma)$ denote the log pdf of $\mathcal{N}(\mu, \sigma^2)$.

The analytic form of $U(x)$ for *ring* is:

$$U(x) = \frac{(\sqrt{x_1^2 + x_2^2} - 2)^2}{0.32} \quad (17)$$

The analytic form of $U(x)$ for *mog2* is:

$$U(x) = f(x|\mu_1, \sigma_1) + f(x|\mu_2, \sigma_2) - \log 2 \quad (18)$$

where $\mu_1 = [5, 0]$, $\mu_2 = [-5, 0]$, $\sigma_1 = \sigma_2 = [0.5, 0.5]$.

The analytic form of $U(x)$ for *mog6* is:

$$U(x) = \sum_{i=1}^6 f(x|\mu_i, \sigma_i) - \log 6 \quad (19)$$

where $\mu_i = [\sin \frac{i\pi}{3}, \cos \frac{i\pi}{3}]$ and $\sigma_i = [0.5, 0.5]$.

The analytic form of $U(x)$ for *ring5* is:

$$U(x) = \min(u_1, u_2, u_3, u_4, u_5) \quad (20)$$

where $u_i = (\sqrt{x_1^2 + x_2^2} - i)^2 / 0.04$.

E.3 Benchmarking Running Time

Since the runtime results depends on the type of machine, language, and low-level optimizations, we try to make a fair comparison between HMC and A-NICE-MC on TensorFlow [38].

Our code is written and executed in TensorFlow 1.0. Due to the optimization of the computation graphs in TensorFlow, the wall-clock time does not seem to be exactly linear in some cases, even when we force the program to use only 1 thread on the CPU. The wall-clock time is affected by 2 aspects, batch size and number of steps. We find that the wall-clock time is relatively linear with respect to the number of steps, and not exactly linear with respect to the batch size.

Given a fixed number of steps, the wall-clock time is constant when the batch size is lower than a threshold, and then increases approximately linearly. To perform speed benchmarking on the methods, we select the batch size to be the value around the threshold, in order to prevent significant under-estimates of the efficiency.

We found that the graph is much more optimized if the batch size is determined before execution. Therefore, we perform all the benchmarks on the optimized graph where we specify a batch size prior to running the graph. For the energy functions, we use a batch size of 2000; for Bayesian logistic regression we use a batch size of 64.

E.4 Hyperparameters for the Energy Function Experiments

For all the experiments, we use same hyperparameters for both A-NICE-MC and HMC. We sample $x_0 \sim \mathcal{N}(0, I)$ and run the chain for 1000 burn-in steps and evaluate the samples from the next 1000 steps.

For HMC we use 40 leapfrog steps and a step size of 0.1. For A-NICE-MC we consider $f_\theta(x, v)$ with three coupling layers, which updates v , x and v respectively. The motivation behind this particular architecture is to ensure that both x and v could affect the updates to x' and v' . In each coupling layer, we select the function $m(\cdot)$ to be a one-layer NN with 400 neurons. The discriminator is a three layer MLP with 400 neurons each. Similar to the settings in Section 3.1, we use the gradient penalty method in [17] to train our model.

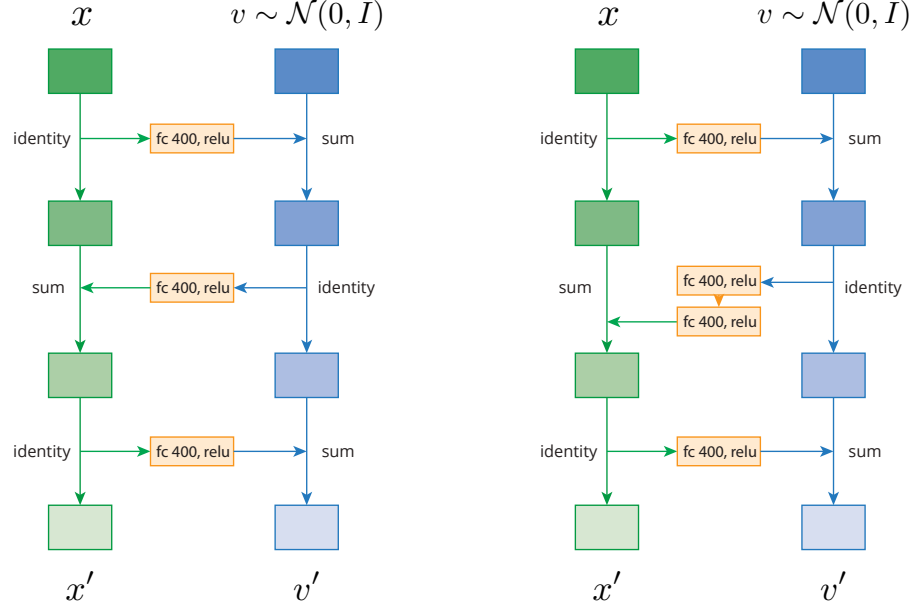
For bootstrapping, we first collect samples by running the NICE proposal over the untrained f_θ , and for every 500 iterations we replace half of the samples with samples from the latest trained model. All the models are trained with AdaM [39] for 20000 iterations with $B = 4$, $M = 2$, batch size of 32 and learning rate of 10^{-4} .

E.5 Hyperparameters for the Bayesian Logistic Regression Experiments

For HMC we tuned the step size parameter to achieve the best ESS possible on each dataset, which is 0.005 for *german*, 0.01 for *heart* and 0.0115 for *australian* (HMC performance on *australian* is extremely sensitive to the step size). For A-NICE-MC we consider $f(x, v)$ with three coupling layers, which updates v , x and v respectively; we set v to have 50 dimensions in all the experiments. $m(\cdot)$ is a one-layer NN with 400 neurons for the top and bottom coupling layer, and a two-layer NN with 400 neurons each for the middle layer. The discriminator is a three layer MLP with 800 neurons each. We use the same training and bootstrapping strategy as in Appendix E.4. All the models are trained with AdaM for 20000 iterations with $B = 16$, $M = 2$, batch size of 32 and learning rate of 5×10^{-4} .

E.6 Architecture Details

The following figure illustrates the architecture details of $f_\theta(x, v)$ for A-NICE-MC experiments. We do not use batch normalization (or other normalization techniques), since it slows the execution of the network and does not provide much ESS improvement.



F Extended Images

We only displayed a small number of images in the main text due to limited space. Here we include the extended version of images for our image generation experiments.

F.1 Extended Images for Figure 1

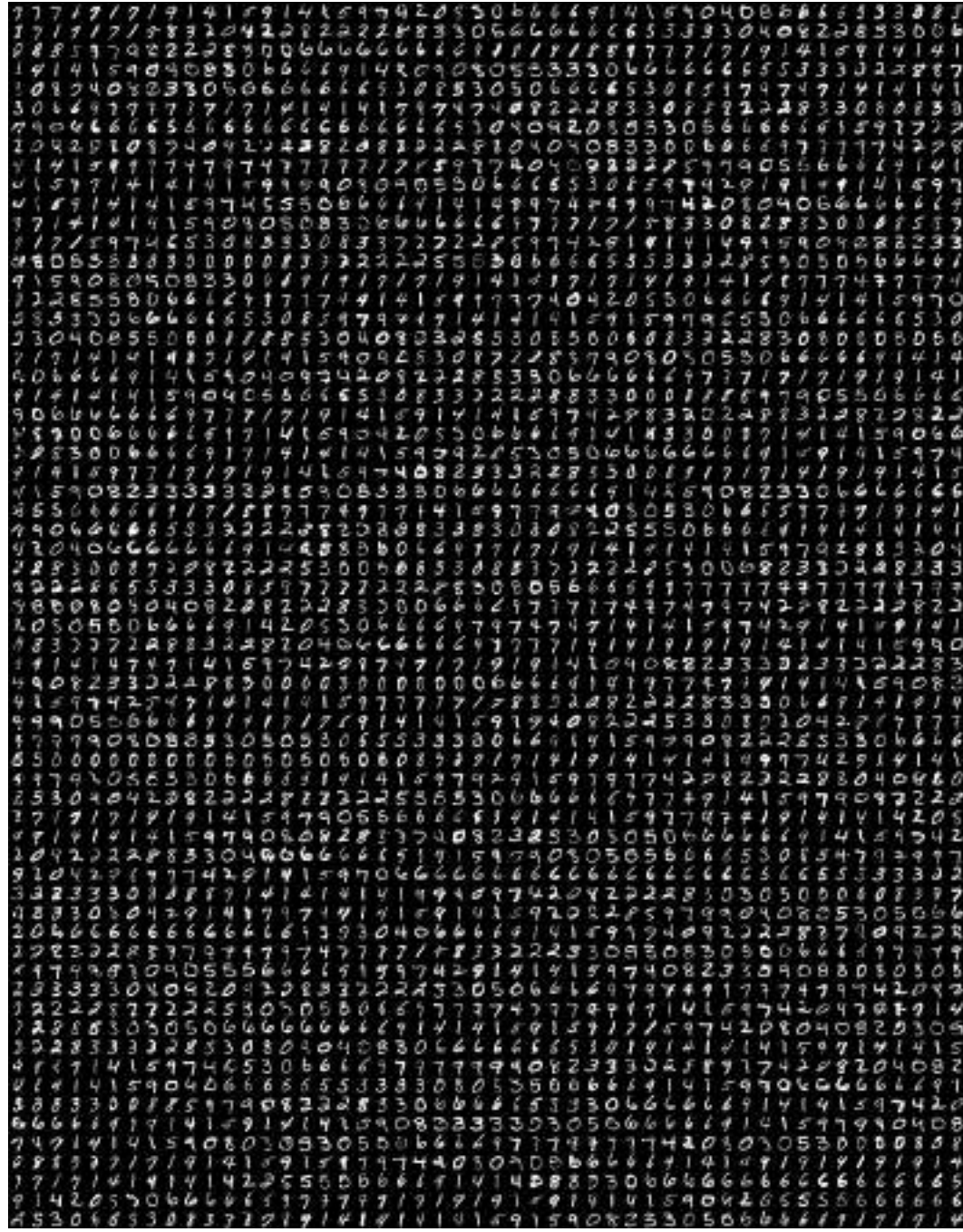


Figure 11: Samples from π_1 to π_{50} from a model trained on the MNIST dataset. Each row are samples from the same chain.

F.2 Extended Images for Figure 3

The following models are trained with the original MGAN objective (without pairwise discriminator).

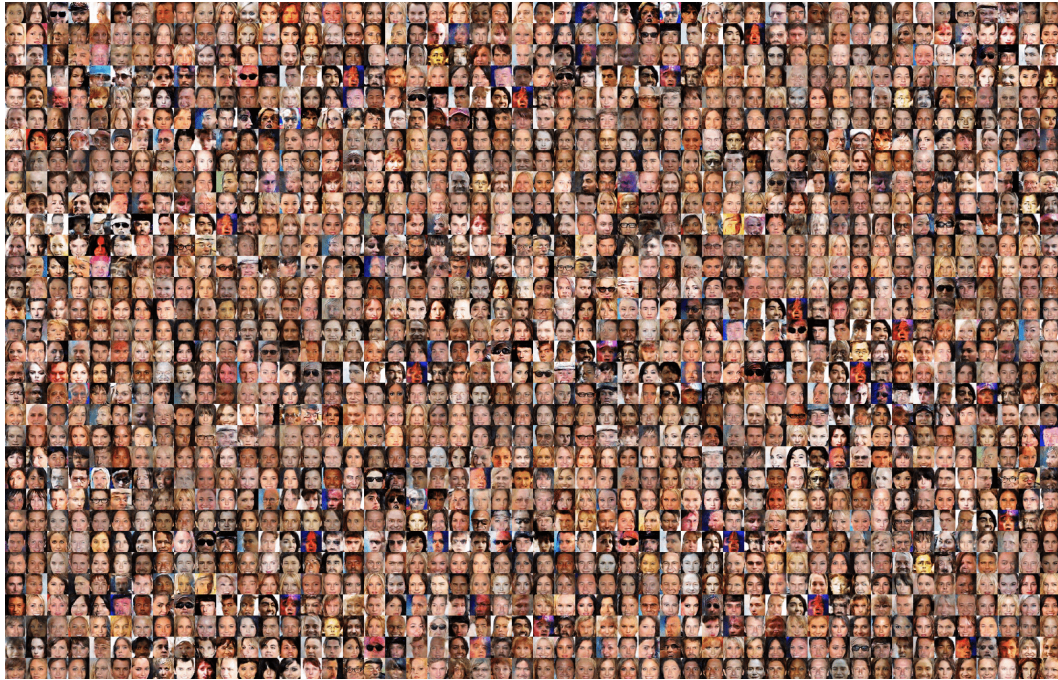


Figure 12: Samples from π_1 to π_{50} from a model trained on the CelebA dataset. Each row are samples from the same chain.



Figure 13: Samples from π_1 to π_{50} from a model trained on the CelebA dataset, where the model has shortcut connections. Each row are samples from the same chain.

F.3 Extended Images for Figure 5

The following images are trained on the same model with shortcut connections.

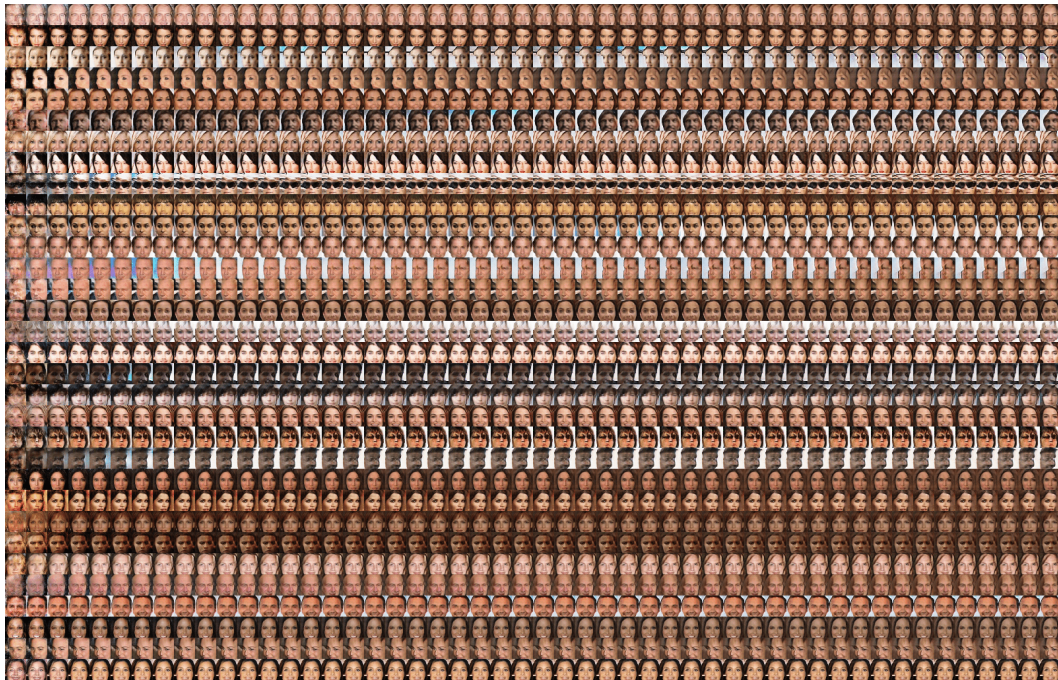


Figure 14: Samples from π_1 to π_{50} from a model trained on the CelebA dataset without pairwise discriminator. Each row are samples from the same chain.

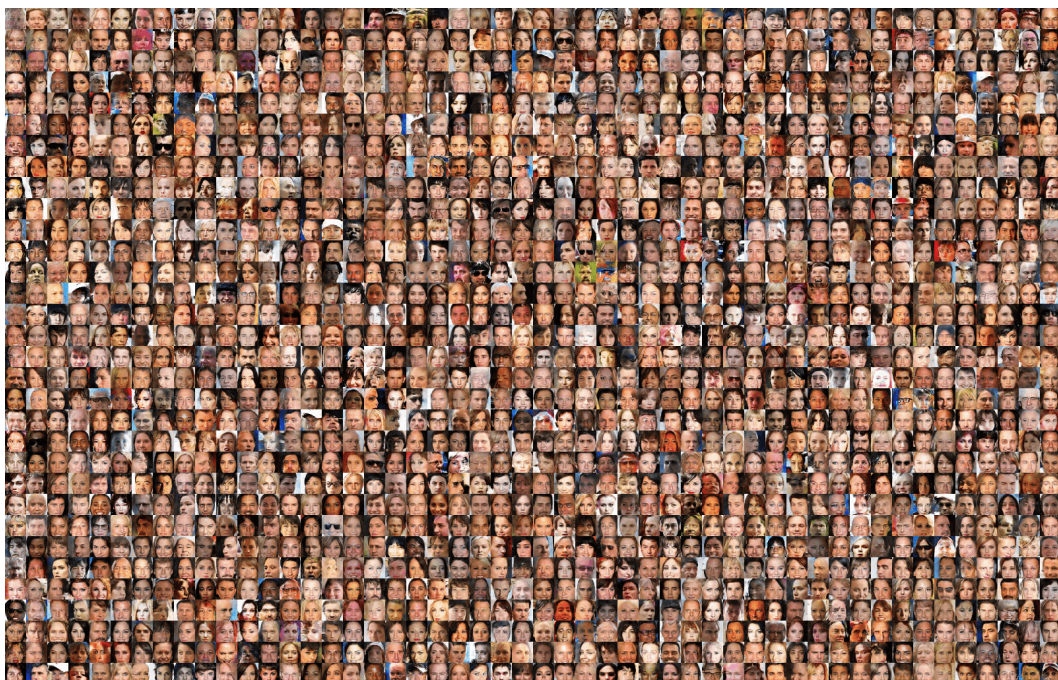


Figure 15: Samples from π_1 to π_{50} from a model trained on the CelebA dataset with pairwise discriminator. Each row are samples from the same chain.